

Acoustic Phonon Tunneling and Heat Transport due to Evanescent Electric Fields

Mika Prunnila* and Johanna Meltaus

VTT Technical Research Centre of Finland, P.O.Box 1208, FIN-02044 VTT, Espoo, Finland

(Dated: February 4, 2022)

The authors describe how acoustic phonons can directly tunnel through vacuum and, therefore, transmit energy and conduct heat between bodies that are separated by a vacuum gap. This effect is enabled by introducing a coupling mechanism, such as piezoelectricity, that strongly couples electric field and lattice deformation. The electric field leaks into the vacuum as an evanescent field, which leads to finite solid-vacuum-solid transmission probability. Due to strong resonances in the system some phonons can go through the vacuum gap with (or close to) unity transmission, which leads to significant thermal conductance and heat flux.

PACS numbers: 44.10.+i, 63.22.Np, 63.22.-m, 77.84.-s
Keywords:

The heat flux of thermally excited photons from an ideal black body at a temperature T is given by the Stefan-Boltzmann law, which states that the flux is proportional to T^4 . The net flux between two black bodies, which are at different temperature and separated by a large vacuum gap d , is the difference of their individual Stefan-Boltzmann fluxes. When a realistic emissivity/absorption is considered this T^4 power law is altered, but the essential physics still remains the same. However, when d is smaller than the characteristic wave length λ_T of thermal spectrum various near-field radiation effects start to play crucial role in the inter-body heat transport and new physics emerges (see Refs. [1, 2] for a review). In this $qTd < 1$ limit ($qT = 2\pi/\lambda_T$ being the thermal wave vector) the heat flux is enhanced particularly by evanescent waves, as explained correctly first by Polder and Van Hove [3]. Recent advances in experimental techniques have enabled near-field heat transfer measurements from μm down to 10 nm body distances.[4–6] In this Letter, we propose that at such distances a new type of evanescent field heat transfer mechanism due to acoustic phonons can exist.

Even though acoustic phonons are the major heat carriers in dielectrics, their effect on heat transfer through a vacuum gap has been considered to be negligible, because they couple weakly to photons. Here we demonstrate by theoretical means that significant energy transmission and heat flux is possible if the acoustic phonons can induce an electric field, which then can leak into the vacuum [see Figs. 1(a) and (b)]. Such a mechanism is provided, for example, by the density response of free carriers due to phonons or by the piezoelectric (PE) effect. Here we shall focus on the latter, which gives rise to a strong coupling between phonon induced material deformation and macroscopic electric fields. The solid-vacuum-solid transmission phenomenon described here can be thought of as an acoustic phonon tunneling through vacuum.

We consider a system in which two phonon black bodies 1' and 3', which serve as fully thermalizing reservoirs, are connected to bodies 1 and 3, which serve as wave guides for the propagating acoustic phonons [Fig. 1(a)]. The propagating modes hit the solid-vacuum interfaces and produce the evanescent electric fields of interest [Fig. 1(b)], which lead to non-zero solid-vacuum-solid energy transmission coefficient $\mathcal{T}_\gamma = \sum_\mu \mathcal{T}_{\mu\gamma}$ for incident mode $\gamma = L, S$. Mode indices L and S stand for longitudinal and transversal, respectively (the two transversal modes are not written explicitly). The energy transmission probability $\mathcal{T}_{\mu\gamma} = \mathcal{T}_{\mu\gamma}(qd, \theta)$ (from mode γ to mode μ) is a function of the phonon polarizations, the absolute value of the incident phonon wavevector q and the angle of incidence θ . Now, following Ref. [7] the thermal boundary conductance G_γ arising from transmission of mode γ can be defined as

$$G_\gamma = \int_{v_z > 0} \frac{d^3q}{(2\pi)^3} \hbar \omega_{\mathbf{q}} \frac{\partial N(\omega_{\mathbf{q}}, T)}{\partial T} v_\gamma \mathcal{T}_\gamma$$

$$= \frac{2\pi^2}{30} v_\gamma k_B q_T^3 \left(1 + \frac{q_T}{4} \frac{\partial}{\partial q_T} \right) \mathcal{T}_\gamma^{eff} \quad (1a)$$

$$\mathcal{T}_\gamma^{eff} = \frac{15}{\pi^4} \left\langle \int_0^{q_c/q_T} dx \frac{x^3}{e^x - 1} \mathcal{T}_\gamma \right\rangle, \quad (1b)$$

where \mathcal{T}_γ^{eff} is the effective energy transmission coefficient. The total thermal conductance and net heat flux are given by $G = \sum_\gamma G_\gamma$ and $P = \int_{T_3}^{T_1} G dT$, respectively. Temperature dependency arises from phonon occupation number $N(\omega_{\mathbf{q}}, T) = [\exp(\hbar\omega_{\mathbf{q}}/k_B T) - 1]^{-1}$ and in \mathcal{T}_γ^{eff} the temperature is buried into the thermal wave vector $q_T = 2\pi/\lambda_T = k_B T/\hbar v_\gamma$ (λ_T is the thermal phonon wave length and v_γ is the phonon velocity). For the sake of simplicity we have assumed a linear dispersion $\omega_{\mathbf{q}} = v_\gamma q$ in Eq. (1b). The parameter $q_c \sim 1/a$ is the Brillouin/Debye cut-off (a being the lattice constant). The bracket $\langle \dots \rangle$ stands for a solid angle average over half-space. Note that if $\mathcal{T}_\gamma = 1$ and $\frac{q_c}{q_T} \rightarrow \infty$, then $\mathcal{T}_\gamma^{eff} = 1$ and P is equal to the phonon black-body flux.

*Electronic address: mika.prunnila@vtt.fi

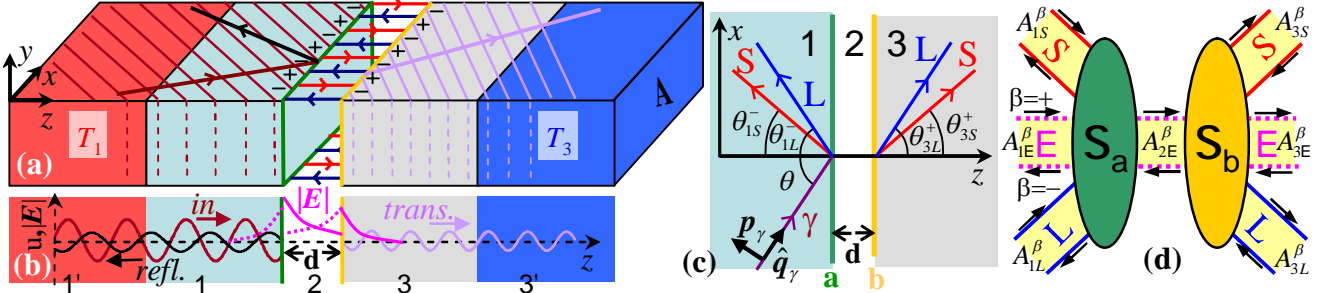


FIG. 1: (Color online) Illustration of the phonon tunneling effect caused by evanescent electric fields. (a) Cross-sectional slice of area A illustrating a phonon incoming from a thermal path 1' at temperature T_1 and hitting a solid-vacuum interface. The phonon carries an electric field, illustrated by \pm signs of polarization in between the wave fronts. The polarization induces an electric field into the vacuum gap 2 (some field lines illustrated). The field enables finite transmission over the gap into the thermal bath 3' (at temperature T_3). The wave fronts of the reflected phonon are not shown. (b) A projection along the z -axis showing the spatial behaviour of the phonon waves (u) and of the evanescent electric field ($\mathbf{E} = \mathbf{E}_E$). The dashed curves depict the "reflected" evanescent field. (c) Illustration of the scattering of the incoming mode γ into different propagating modes (L =longitudinal and S =transversal). $\hat{\mathbf{q}}_\gamma$ and \mathbf{p}_γ are the propagation and polarization vectors, respectively. (d) The scattering matrix formulation of the problem (See Eq. 2).

The energy transmissions are calculated from the scattering matrices (S-matrix) \mathcal{S}_i ($i = a, b$) of the two solid-vacuum interfaces a and b . We define \mathcal{S}_i in such a way that it couples the amplitudes $A_{\alpha\nu}^\beta$ of propagating fields and exponentially decaying near-fields [see Fig. 1(d)]. Here, $\beta = \pm$, where $+$ ($-$) refers to left-to-right (right-to-left) propagating or decaying wave, $\alpha = 1, 2, 3$ is the material index (2 referring to the vacuum gap), and ν is the mode/channel index ($\nu = E$ refers to the evanescent channel). For example, for the interface a we write

$$\begin{pmatrix} A_{1L}^- \\ A_{1S}^- \\ A_{1E}^- \\ A_{2E}^+ \end{pmatrix} = \mathcal{S}_a \begin{pmatrix} A_{1\gamma}^+ \\ A_{2E}^- \end{pmatrix} = \begin{pmatrix} r_a & t'_a \\ 3 \times 1 & 3 \times 1 \\ t_a & r'_a \\ 1 \times 1 & 1 \times 1 \end{pmatrix} \begin{pmatrix} A_{1\gamma}^+ \\ A_{2E}^- \end{pmatrix}. \quad (2)$$

The labels of the sub-matrices r_a , t'_a , t_a and r'_a indicate the size of these matrices. We assume that in all materials there is only one channel that arises from evanescent electric fields. This fully covers the case in which we neglect all retardation effects and utilize the quasistatic approximation. Now, $A_{\alpha E}^\beta$ is more conveniently related to the evanescent potential Φ_E instead of the evanescent electric field \mathbf{E}_E ($\mathbf{E}_E = -\nabla\Phi_E$). The amplitudes $A_{\alpha E}^\beta$ are coupled to the acoustic amplitudes if an acoustic phonon creates a periodic charge density or polarization, which then creates an evanescent field/potential due to a boundary. The retardation effects become important if the oscillation period of the surface polarization (arising from the acoustic phonons) is of the order of the time it takes light to make a round trip across the gap. This leads to cut-off energy $\mathcal{E}_c = hc/2d \approx 620 \text{ meV} \times (\mu\text{m}/d)$, below which our model is valid. Note that \mathcal{E}_c is above acoustic phonon energies when $d < 10 \mu\text{m}$.

For the full solid-vacuum-solid system we need to find the total S-matrix $\mathcal{S} = \mathcal{S}_a \otimes \mathcal{S}_b$ that couples the ampli-

tudes of the different solids. From \mathcal{S} we specifically need the sub-matrix t , which describes the amplitude transmission. By solving $\mathcal{S} = \mathcal{S}_a \otimes \mathcal{S}_b$ and taking into account the exponential factors arising from the finite distance d we find

$$t_{\mu\gamma} = \{t'_b\}_\mu [1 - e^{-2\eta qd} r'_a r'_b]^{-1} \{t_a\}_\gamma e^{-\eta qd}, \quad (3)$$

where we have inverted the z -axis for \mathcal{S}_b so that \mathcal{S}_a and \mathcal{S}_b have a similar structure. Here the evanescent field is excited by the oscillating polarization perpendicular to the z -axis and, therefore, we have $\eta = |\sin\theta|$. The energy transmission coefficients are given by $\mathcal{T}_{\mu\gamma} = \alpha_{\mu\gamma} |t_{\mu\gamma}|^2$, where $\alpha_{\mu\gamma}$ is a factor that converts the amplitude transmission into energy transmission probability. We write the total energy transmission $\mathcal{T}_\gamma = \sum_\mu \mathcal{T}_{\mu\gamma}$ in the form

$$\mathcal{T}_\gamma = \frac{e^{2\eta qd}}{(e^{2\eta qd} - R)^2 + I^2} \sum_\mu \mathcal{A}_{\mu\gamma}, \quad (4)$$

where $\mathcal{A}_{\mu\gamma} = \alpha_{\mu\gamma} |\{t'_b\}_\mu \{t_a\}_\gamma|^2$, $R = \text{Re}\{r'_a r'_b\}$ and $I = \text{Im}\{r'_a r'_b\}$. $\alpha_{\mu\gamma}$ can be determined from the acoustic Poynting vector [8] and in the simplest case of isotropic solid we have $\alpha_{\mu\gamma} = \frac{\rho_3 v_\mu}{\rho_1 v_\gamma} \text{Re}\{\hat{\mathbf{q}}_\mu\}_z$, where ρ_i is the mass density of material i and $\{\hat{\mathbf{q}}_\mu\}_z = (1 - (v_\mu^2/v_\gamma^2) \sin^2\theta)^{1/2}$ is the z -direction propagation vector.

Our next task is to calculate the energy transmission coefficient \mathcal{T}_γ in the case of two similar PE crystals separated by a vacuum gap. In such a piezoacoustic system, we are dealing with coupled acoustic and electromagnetic fields. Within the quasistatic model, the relevant field quantities (see Table I) and their couplings are defined

TABLE I: Field quantities and constants.

Symbol	Size	Name
\mathbf{T}	6×1	Stress
$\hat{\mathbf{e}}$	3×6	Piezo tensor
Φ	1×1	Potential
$\hat{\mathbf{c}}$	6×6	Stiffness tensor
\mathbf{u}	3×1	Lattice displacement
\mathbf{D}	3×1	Electric displacement
$\hat{\mathbf{e}}$	3×3	Dielectric constant

by [8]

$$\mathbf{T} = \hat{\mathbf{e}}^T \nabla \Phi + \hat{\mathbf{c}} \nabla_u \mathbf{u} \quad (5a)$$

$$\mathbf{D} = -\hat{\mathbf{e}} \nabla \Phi + \hat{\mathbf{e}} \nabla_u \mathbf{u} \quad (5b)$$

$$\nabla^T \hat{\mathbf{e}} \nabla \Phi = \nabla^T \hat{\mathbf{c}} \nabla_u \mathbf{u}, \quad (5c)$$

where $\nabla = [\partial/\partial x, \partial/\partial y, \partial/\partial z]^T$ and ∇_u is the displacement-to-strain operator (6×3 matrix). The form of the operator ∇_u follows from the relation $\epsilon_{\alpha\beta} = \frac{1}{2}(\partial u_\alpha/\partial \beta + \partial u_\beta/\partial \alpha)$ ($\alpha, \beta = x, y, z$), which couples the six symmetric strain components $\epsilon_{\alpha\beta}$ to the components of displacement \mathbf{u} . Note that Eq. (5c) is basically a Poisson equation and the source term $\nabla^T \hat{\mathbf{e}} \nabla_u \mathbf{u}$ gives rise to the phonon induced evanescent electric fields. The S-matrices \mathcal{S}_i are solved from a boundary condition equation that is obtained by requiring the continuity of the potential Φ , the normal component of electric displacement \mathbf{D} and the normal component of stress \mathbf{T} at the interfaces. The boundary condition equation and the resulting \mathcal{S}_i are given in the supplementary material [9]. We calculate \mathcal{T}_γ [Eq. (4)] by solving the S-matrix numerically. We adopt material parameters that are close to that of ZnO [8] with the simplifying approximation $\{\hat{\mathbf{e}}\}_{ij} = \delta_{3j}\delta_{i3}e_{33}$, where $e_{33} = 1.3$ C/m². Furthermore, we assume that the acoustic properties are isotropic and that the PE stiffening can be neglected for the propagating modes. These assumptions have very little effect on the angular averaged quantities of interest (\mathcal{T}_γ^{eff} and G_γ). We use isotropic values $c_{11} = 209.7 \times 10^9$ N/m², $c_{44} = 42 \times 10^9$ N/m² and $\{\hat{\mathbf{e}}\}_{ij} = 10\epsilon_0\delta_{ij}$. The phonon velocities are given by $v_L = \sqrt{c_{11}/\rho} = 6119.3$ m/s and $v_S = \sqrt{c_{44}/\rho} = 2738.6$ m/s, where the mass density $\rho = 5600$ kg/m³.

Figure 2 shows $\mathcal{T}_\gamma(qd, \theta)$ for phonon tunneling from a PE material to another across a vacuum gap. There are two local minima in \mathcal{T}_S : one at $\theta \approx 25^\circ$ and another one at $\theta \approx 40^\circ$. The position of the latter minima can be related to the phase change of the evanescent electric field in the vacuum-solid reflection. The former minima is the critical incidence angle where the quasi-longitudinal surface mode is exited. Most important effects for the energy transmission are the strong resonance features for both modes: for some (qd, θ) -values \mathcal{T}_γ is very large or even equal to unity. The resonances arise from the multiple reflections of the evanescent field in the vacuum gap, which leads to the $[(e^{2\eta qd} - R)^2 + I^2]^{-1}$ factor in \mathcal{T}_γ [see

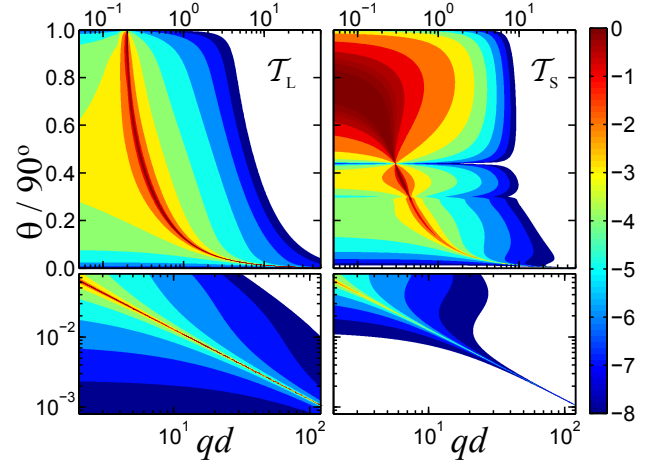


FIG. 2: (Color online) Logarithmic contour plot of energy transmission coefficients \mathcal{T}_γ ($\gamma = L, S$) between two PE bodies as a function of normalized wave vector qd and the angle of incidence θ . White regions have $\mathcal{T}_\gamma < 10^{-8}$. The lower panels show log-log blow-up of the small- θ large- qd region.

Eq. (4)]. The elements $r'_{a,b}$ are dictated by the vacuum-solid boundary conditions and their real parts or moduli are not limited below unity. Thus we may have $R > 1$ and $I \ll 1$, which leads to a sharp resonance peak at $2\eta qd = \ln R$. Indeed, for $\gamma = L$, we have $R \sim 1.5$ for all incident angles and this is the origin of the sharp maximum trajectory in $\mathcal{T}_L(qd, \theta)$. For $\gamma = S$, $R > 1$ only for angles $\theta < 68^\circ$, and above this threshold no sharp resonances exist. For small θ at $qd \gg 1$, $\mathcal{T}_L = 1$ at the resonance, whereas the amplitude of the resonance peak in \mathcal{T}_S decays as a function of qd (see the lower panels of Fig. 2). Note that the phonon resonant tunneling here has a striking similarity to the resonant photon tunneling described, for example, in Ref. [2].

Inserting the calculated \mathcal{T}_γ into Eq. (1) and performing numerical integration, we obtain \mathcal{T}_γ^{eff} and G_γ . The results are presented in Fig. 3. We observe that at low temperatures when $qTd \ll 1$ the effective transmission \mathcal{T}_S^{eff} is $\sim 15\%$ of the unity transmission resulting in relatively large G_S , which is of the order of the maximum possible thermal conductance allowed by Eq. (1a). The large \mathcal{T}_S^{eff} at low temperatures follows from the broadened resonances and from the large transmission amplitude for the S -mode for large θ and small qd (see Fig. 2). For $\gamma = L$ we have sharp resonances leading to a small effective transmission and to $G_L \ll G_S$ at low temperatures.

Next, we want to investigate the dependency of \mathcal{T}_γ^{eff} on qTd and the contribution of different phonons in the (qd, θ) phase space to the heat transport. We divide \mathcal{T}_γ^{eff} into small angle $\mathcal{T}_{\gamma, \theta < \theta_{th}}^{eff}$ and large angle $\mathcal{T}_{\gamma, \theta > \theta_{th}}^{eff}$ contributions:

$$\mathcal{T}_\gamma^{eff} = \mathcal{T}_{\gamma, \theta < \theta_{th}}^{eff} + \mathcal{T}_{\gamma, \theta > \theta_{th}}^{eff}, \quad (6)$$

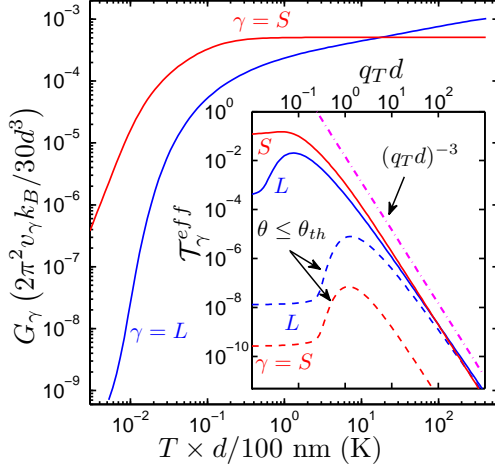


FIG. 3: (Color online) Heat transport between two PE bodies: effective transmission \mathcal{T}_γ^{eff} (the inset) as a function of qTd and the interface thermal conductance G_γ (the main part) as a function of temperature. The curves are obtained from the \mathcal{T}_γ of Fig. (2) and Eq. (1) (we have set $q_c/q_T \rightarrow \infty$). The dashed curves in the inset are small angle contributions $\mathcal{T}_{\gamma,\theta < \theta_{th}}^{eff}$ with $\theta_{th} = 3^\circ$. The dot-dash curve indicates $(qTd)^{-3}$ slope. For the y-axis units of the main Figure we have $2\pi^2 v_\gamma k_B / 30d^3 = Y_\gamma \times (100 \text{ nm}/d)^3 \text{ W/Km}^2$, where $Y_{L(S)} = 55.6$ (24.9).

where the angular integrals of the different contributions are limited by the threshold θ_{th} , which is chosen in such away that major contribution to $\mathcal{T}_{\gamma,\theta < \theta_{th}}^{eff}$ comes from the resonance trajectory at $qd > 1$. The exact choice of θ_{th} is, therefore, somewhat arbitrary and in the numerical calculations we define $\theta_{th} = 3^\circ$, whence $\theta < \theta_{th}$ roughly correspond to the phase space of the lower panels of Fig. 2. At the high temperature limit ($qTd \gg 1$), small and large angle effective transmissions can be written as[9]

$$\mathcal{T}_{\gamma,\theta < \theta_{th}}^{eff} \approx \sum_\mu \frac{15}{\pi^3} \frac{[\ln R(0)]^{n+1}}{(2qTd)^{2+n}} \times \frac{f_{\mu\gamma}^n(0)}{n!} F_n\left(\frac{q_c}{q_T}, \theta_{th}\right) \quad (7a)$$

$$\mathcal{T}_{\gamma,\theta > \theta_{th}}^{eff} \approx \frac{15}{\pi^4} \frac{1}{(qTd)^3} \left\langle \int_0^{q_c d} dy y^2 \mathcal{T}_\gamma(y, \theta) \right\rangle_{\theta \geq \theta_{th}}, \quad (7b)$$

where $F_n(\frac{q_c}{q_T}, \theta_{th}) = \int_{x_{th}}^{q_c/q_T} dx \frac{x^{1-n}}{\exp(x)-1}$ with $x_{th} = \ln R(\theta_{th}) / (2qTd \sin \theta_{th})$, $f_{\mu\gamma}^n(\theta) = \mathcal{A}_{\mu\gamma}(\theta) / I(\theta)$ and $f_{\mu\gamma}^n(\theta)$ is the first non-zero derivative of $f_{\mu\gamma}(\theta)$. Due to the decay of the resonance for the S-mode, $\mathcal{T}_{S,\theta < \theta_{th}}^{eff}$ is very small. This means that practically all contribution to \mathcal{T}_S^{eff} and G_S at any temperature comes from the large angle part $\mathcal{T}_{S,\theta > \theta_{th}}^{eff}$. At high temperatures, $\mathcal{T}_{\gamma,\theta > \theta_{th}}^{eff}$ is given by Eq. (7b), which explains the $(qTd)^{-3}$ fall-off of \mathcal{T}_S^{eff} and the saturation of $G_S \rightarrow G_S^{sat}$ in Fig. 3. The

saturation value $G_S^{sat} = \frac{k_B v_S}{4\pi^2 d^3} \left\langle \int_0^{q_c d} dy y^2 \mathcal{T}_\gamma(y, \theta) \right\rangle_{\theta \geq \theta_{th}}$ follows from Eqs. (7b) and (1a). For the L-mode the high temperature \mathcal{T}_γ^{eff} has also a large contribution arising from $\mathcal{T}_{L,\theta < \theta_{th}}^{eff}$. This contribution eventually exceeds the large angle part and, as a result, there is no saturation in G_L . Close to $\theta = 0$, $\mathcal{T}_{L,\theta < \theta_{th}}^{eff}$ is dominated by $f_{LL}^1(\theta)$, and by setting $\frac{q_c}{q_T} \rightarrow \infty$ in Eq. (7a), we find that $\mathcal{T}_{L,\theta < \theta_{th}}^{eff} \propto (qTd)^{-3} \sum_{k=1}^{\infty} \frac{\exp(-k x_{th})}{k}$, resembling a $(qTd)^{-5/2}$ behavior. It should be noted that the temperature dependency of the large angle contribution is not affected by the ratio q_c/q_T . As q_c^{-1} is of the order of the lattice constant a , Eq. (7b) is valid if $d > a$. The small angle contribution depends on q_c/q_T . For example, if $q_c/q_T \ll 1$, then $\mathcal{T}_{L,\theta < \theta_{th}}^{eff} \propto (qTd)^{-3} \ln \left[\frac{2q_c d \sin \theta_{th}}{\ln R(\theta_{th})} \right]$. Thus, G_L also saturates when the cut-off q_c is exceeded.

At this point we summarize our findings: We have formulated the thermal boundary conductance of a solid-vacuum-solid system [Eq. (1)] using an acoustic phonon energy transmission probability [Eq. (4)] given by scattering matrix [Eq. (2)], which couples the different solids by an evanescent channel produced by phonon induced electric fields (Fig. 1). These fields can lead to a significant energy transmission probability for some parts of the wave vector-angle of incidence (qd, θ) phase space (Fig. 2). The transmission exhibits resonances, which arise from the multiple reflections of the evanescent field in the vacuum gap. The L-mode shows a strong and sharp resonance trajectory across the (qd, θ) -plane with a unity energy transmission probability. The resonance trajectory approaches $\theta = 0$ as $qd \rightarrow \infty$. The S-mode exhibits similar features. However, for a small qd and a large θ the resonance is broadened and in the $qd \gg 1$ limit the energy transmission decays rapidly. At low temperatures ($qTd < 1$), the broadened resonance at small qd leads to a large contribution from the S-mode to the thermal conductance ($\sim 15\%$ of the maximum possible thermal conductance defined by unity transmission). The small qd / large θ part of the phase space dominates the S-mode heat transport leading to a saturation of the thermal conductance of the S-mode at high temperatures (Fig. 3). If the thermal phonon wave length λ_T is sufficiently smaller than the lattice constant, the L-mode shows no such saturation. This is due to the strong resonance in the transmission that persists even at $qd \gg 1$ and, therefore, allows short wave length phonons to go through the vacuum gap. Note that our method to calculate the thermal conductance is essentially similar to that adopted in (ballistic) thermal boundary resistance calculations [7], which means that the thermal excitation of local acusto-electric modes related to the solid-vacuum boundaries is not taken into account. Here, the boundary effects and the evanescent fields are solely due to radiation of bulk acoustic phonons. One can also explicitly take into account thermal excitation and couplings of the local modes, expected to enhance the interbody coupling and the thermal conductance. This approach,

typically adopted in photon near-field studies[1, 2], will be left for future investigations.

Acoustic phonon heat transfer through vacuum can be experimentally verified with direct thermal conductance measurements, using piezoelectric materials. The transmission of acoustic energy across a vacuum gap at long wave lengths can be investigated by measuring the transmission of a single acoustic wave by utilizing, for example, surface acoustic wave devices. Finally, we note that the effects described in this paper can also contribute to the thermal conductivity of polycrystalline piezoelectric materials and percolation systems consisting of piezoelectric particles. Furthermore, as free electrons couple strongly

to electric fields, a similar heat transport effect, that is discussed in this Letter, can also occur between metallic and piezoelectric bodies.

Acknowledgments

We acknowledge useful discussions with P.-O. Chappuis, B. Djafari-Rouhani, J. Ahopelto and T. Pensala. This work was financially supported by EC through the project #216176 NANOPACK.

-
- [1] K. Joulain, J.-P. Mulet, F. Marquier, R. Carminati, and J.-J. Greffet, *Surface Science Reports* **57**, 59 (2005).
 - [2] A. I. Volokitin and B. N. J. Persson, *Rev. Mod. Phys.* **79**, 1291 (2007).
 - [3] D. Polder and M. Van Hove, *Phys. Rev. B* **4**, 3303 (1971).
 - [4] A. Kittel, W. Müller-Hirsch, J. Parisi, S.-A. Biehs, D. Reddig, and M. Holthaus, *Phys. Rev. Lett.* **95**, 224301 (2005).
 - [5] A. Narayanaswamy, S. Shen, and G. Chen, *Phys. Rev. B* **78**, 115303 (2008).
 - [6] E. Rousseau, A. Siria, G. Jourdan, S. Volz, F. Comin, J. Chevrier, and J.-J. Greffet, *Nature Photonics* **3**, 514 (2009).
 - [7] E. T. Swartz and R. O. Pohl, *Rev. Mod. Phys.* **61**, 605 (1989).
 - [8] B. A. Auld, *Acoustic Fields and Waves in Solids I & II* (Krieger, Florida, 1990), 2nd ed.
 - [9] EPAPS Document No. XXX. For more information on EPAPS, see <http://www.aip.org/pubservs/epaps.html>.
-

SUPPLEMENTARY MATERIAL

I. DERIVATION OF THE SCATTERING MATRIX IN A PIEZOACOUSTIC SOLID-VACUUM PROBLEM

In the quasi-static approximation, the piezoelectric constitutive relations for stress \mathbf{T} , electric displacement \mathbf{D} and electric potential Φ , generated by a displacement \mathbf{u} , can be written as [8]

$$\mathbf{T} = \hat{\epsilon}^T \nabla \Phi + \hat{c} \nabla_u \mathbf{u} \quad (8a)$$

$$\mathbf{D} = -\hat{\epsilon} \nabla \Phi + \hat{e} \nabla_u \mathbf{u} \quad (8b)$$

$$\nabla^T \hat{\epsilon} \nabla \Phi = \nabla^T \hat{e} \nabla_u \mathbf{u}. \quad (8c)$$

The electric field \mathbf{E} is given by $\mathbf{E} = -\nabla \Phi$. Tensors $\hat{\epsilon}$, \hat{e} and \hat{c} are dielectric permittivity, piezoelectric coupling and stiffness tensors, respectively. Above Equations are written following the abbreviated tensor subscript notation [8]. The field quantities are summarized in the Table I of the main article. Here, we have defined operators ∇ and ∇_u according to

$$\nabla^T = [\partial/\partial x \quad \partial/\partial y \quad \partial/\partial z] \quad (9a)$$

$$\nabla_u^T = \begin{bmatrix} \partial/\partial x & 0 & 0 & 0 & \partial/\partial z & \partial/\partial y \\ 0 & \partial/\partial y & 0 & \partial/\partial z & 0 & \partial/\partial x \\ 0 & 0 & \partial/\partial z & \partial/\partial y & \partial/\partial x & 0 \end{bmatrix}. \quad (9b)$$

For displacement \mathbf{u} with a known wave vector \mathbf{q} , amplitude A and polarization vector \mathbf{p}

$$\mathbf{u} = A \mathbf{p} e^{-j\mathbf{q} \cdot \mathbf{r}}, \quad (10)$$

the above operators can be written as

$$\nabla = -jq \mathbf{L} \quad (11a)$$

$$\nabla_u = -jq \mathbf{L}_u, \quad (11b)$$

where \mathbf{L} and \mathbf{L}_u are defined with the components l_x, l_y and l_z of the unit propagation vector parallel to wave vector \mathbf{q} :

$$\mathbf{L}^T = [l_x \quad l_y \quad l_z] \quad (12a)$$

$$\mathbf{L}_u^T = \begin{bmatrix} l_x & 0 & 0 & 0 & l_z & l_y \\ 0 & l_y & 0 & l_z & 0 & l_x \\ 0 & 0 & l_z & l_y & l_x & 0 \end{bmatrix}. \quad (12b)$$

Re-writing the constitutive relations for $\mathbf{u} = A \mathbf{p} e^{-j\mathbf{q} \cdot \mathbf{r}}$ with \mathbf{L} and \mathbf{L}_u , we get

$$\mathbf{T} = -jq \left[\frac{\hat{\epsilon}^T \hat{e}}{\mathbf{L}^T \hat{\epsilon} \mathbf{L}} + \hat{c}^E \right] \mathbf{L}_u \mathbf{p} \quad (13a)$$

$$\mathbf{D} = jq \left[\hat{\epsilon} \frac{1}{\mathbf{L}^T \hat{\epsilon} \mathbf{L}} \mathbf{L} \mathbf{L}^T - 1 \right] \hat{e} \mathbf{L}_u \mathbf{p} \quad (13b)$$

$$\Phi = \frac{\mathbf{L}^T \hat{e} \mathbf{L}_u \mathbf{p}}{\mathbf{L}^T \hat{\epsilon} \mathbf{L}}, \quad (13c)$$

where we have excluded the amplitude-phase factor $A e^{-j\mathbf{q} \cdot \mathbf{r}}$. The evanescent electric field is described through evanescent potential $\Phi_E = A_E e^{-j\mathbf{q}_\rho \cdot \mathbf{r} + q_e z}$ ($\mathbf{q}_\rho = \mathbf{q}_x + \mathbf{q}_y$), for which similar field relations are given by

$$\mathbf{T}_E = e^T \nabla \Phi_E = -jq e^T \mathbf{L}_E \quad (14a)$$

$$\mathbf{D}_E = -\hat{\epsilon} \nabla \Phi_E = jq \hat{\epsilon} \mathbf{L}_E, \quad (14b)$$

with

$$\mathbf{L}_E^T = [l_x \quad l_y \quad l_E], \quad (15)$$

where $l_E = q_e/jq = \pm |q_\rho|/jq = \pm 1/\sqrt{2}j$.

Boundary conditions at free piezoelectric boundary between materials 1 and 2 (vacuum) require the absence of stresses and the continuation of Φ and the normal component of \mathbf{D} . Thus, we have boundary conditions

$$\mathbf{T}_1 \hat{n}_1 = 0 \quad (16a)$$

$$\mathbf{D}_1 \hat{n}_1^T = \mathbf{D}_2 \hat{n}_2^T \quad (16b)$$

$$\Phi_1 = \Phi_2, \quad (16c)$$

where \hat{n}_α ($\alpha = 1, 2$ and $|\hat{n}_\alpha| = 1$) are the normal vectors of the boundary pointing into material α . Eq. (16a) involves tensor form of \mathbf{T} :

$$\mathbf{T} = \begin{bmatrix} T_1 & T_6 & T_5 \\ T_6 & T_2 & T_4 \\ T_5 & T_4 & T_3 \end{bmatrix}. \quad (17)$$

Now, we include the notation of the main article, which writes the amplitudes as $A_{\alpha\nu}^\beta$, where $\beta = +(-)$ denotes the left-to-right (right-to-left) propagating (or evanescent) wave, α denotes the material, and ν denotes the wave / field mode (L =longitudinal, S =shear, E =evanescent). From Eqs. (13), (14) and (16) we find the boundary condition matrix equation

$$\begin{aligned} & \begin{bmatrix} [\mathbf{T}_{1\gamma}^+ \hat{n}_1] & [\mathbf{T}_{1L}^- \hat{n}_1] & [\mathbf{T}_{1S}^- \hat{n}_1] & [\mathbf{T}_{1E}^- \hat{n}_1] \\ [\mathbf{D}_{1\gamma}^+ \hat{n}_1^T] & [\mathbf{D}_{1L}^- \hat{n}_1^T] & [\mathbf{D}_{1S}^- \hat{n}_1^T] & [\mathbf{D}_{1E}^- \hat{n}_1^T] \\ \Phi_{1\gamma}^+ & \Phi_{1L}^- & \Phi_{1S}^- & \Phi_{1E}^- \end{bmatrix} \begin{bmatrix} A_{1\gamma}^+ \\ A_{1L}^- \\ A_{1S}^- \\ A_{1E}^- \end{bmatrix} \\ &= \begin{bmatrix} [0] & [0] \\ [\mathbf{D}_{2E}^+ \hat{n}_2^T] & [\mathbf{D}_{2E}^- \hat{n}_2^T] \\ \Phi_{2E}^+ & \Phi_{2E}^- \end{bmatrix} \begin{bmatrix} A_{2E}^+ \\ A_{2E}^- \end{bmatrix}. \end{aligned} \quad (18)$$

Here, $A_{1\gamma}^+$ is the amplitude of an incident propagating mode $\gamma = L, S$ in material 1. The acoustic field related elements $\mathbf{T}_{\alpha\nu}^\beta$, $\mathbf{D}_{\alpha\nu}^\beta$, and $\Phi_{\alpha\nu}^\beta$ ($\nu = S, L$) are given by Eqs. (13) and the evanescent field related elements $\mathbf{T}_{\alpha E}^\beta$ and $\mathbf{D}_{\alpha E}^\beta$ are given by Eqs. (14). The elements $\Phi_{\alpha E}^\beta$ are defined by the continuity of the potential and, therefore, $\Phi_{\alpha E}^\beta = 1$. The elements in square brackets (for example

$[\mathbf{T}_{1E}^-\hat{n}_1]$ are not scalars: here $\dim\{[x]\} = 2 \times 1$. From Eq. (18) we obtain the scattering matrix equation

$$\begin{bmatrix} A_{1L}^- \\ A_{1S}^- \\ A_{1E}^- \\ A_{2E}^+ \end{bmatrix} = \mathcal{S} \begin{bmatrix} A_{1\gamma}^+ \\ A_{2E}^- \end{bmatrix}, \quad (19)$$

where the scattering matrix \mathcal{S} is defined by

$$\mathcal{S} = \begin{bmatrix} [\mathbf{T}_{1L}^-\hat{n}_1] & [\mathbf{T}_{1S}^-\hat{n}_1] & [\mathbf{T}_{1E}^-\hat{n}_1] & [0] \\ \mathbf{D}_{1L}^-\hat{n}_1^T & \mathbf{D}_{1S}^-\hat{n}_1^T & \mathbf{D}_{1E}^-\hat{n}_1^T & -\mathbf{D}_{2E}^+\hat{n}_2^T \\ \Phi_{1L}^- & \Phi_{1S}^- & \Phi_{1E}^- & -\Phi_{2E}^+ \end{bmatrix}^{-1} \times \begin{bmatrix} -[\mathbf{T}_{1\gamma}^+\hat{n}_1] & [0] \\ -\mathbf{D}_{1\gamma}^+\hat{n}_1^T & \mathbf{D}_{2E}^-\hat{n}_2^T \\ -\Phi_{1\gamma}^+ & \Phi_{2E}^- \end{bmatrix}. \quad (20)$$

This equation is utilized in solving the S-matrix and the energy transmission in the main article. Note that all \mathbf{q} -vectors $\mathbf{q}_{\alpha\nu}^\beta$ are proportional to the incident mode wave number $q = |\mathbf{q}_{1\gamma}^+|$ and, therefore, \mathcal{S} does not depend on q . Furthermore, as incident mode γ is a parameter of \mathcal{S} we must actually consider \mathcal{S} as a sub-matrix of the total S-matrix.

II. \mathcal{T}_γ^{eff} AT $q_T d \gg 1$ LIMIT

In the main article we divide the effective transmission \mathcal{T}_γ^{eff} into small angle $\mathcal{T}_{\gamma,\theta < \theta_{th}}^{eff}$ and large angle $\mathcal{T}_{\gamma,\theta > \theta_{th}}^{eff}$ contributions:

$$\mathcal{T}_\gamma^{eff} = \mathcal{T}_{\gamma,\theta < \theta_{th}}^{eff} + \mathcal{T}_{\gamma,\theta > \theta_{th}}^{eff}, \quad (21)$$

where the angular integrals of the different contributions are limited by the threshold θ_{th} . We will describe the derivation of the high temperature ($q_T d \gg 1$) analytical formulas of $\mathcal{T}_{\gamma,\theta < \theta_{th}}^{eff}$ and $\mathcal{T}_{\gamma,\theta > \theta_{th}}^{eff}$ below.

A. Small angle contribution $\mathcal{T}_{\gamma,\theta < \theta_{th}}^{eff}$

The energy transmission coefficient is given by (see the main article)

$$\mathcal{T}_\gamma = \frac{e^{2\eta q d}}{(e^{2\eta q d} - R)^2 + I^2} \sum_\mu \mathcal{A}_{\mu\gamma}, \quad (22)$$

where $A_{\mu\gamma} = \alpha_{\mu\gamma} \left| \{t'_b\}_\mu \{t_a\}_\gamma \right|^2$, $R = \text{Re}\{r'_a r'_b\}$ and $I = \text{Im}\{r'_a r'_b\}$. We use approximation ($R > 1$, $I \ll 1$)

$$\frac{1}{(e^{2\eta q d} - R)^2 + I^2} \approx \frac{\pi}{I} \delta(e^{2\eta q d} - R), \quad (23)$$

where $\delta(x)$ is the Dirac delta function. This leads to expression

$$\mathcal{T}_{\mu\gamma} \approx e^{2\eta q d} \frac{\pi}{I} \frac{\delta(\theta - \theta_0)}{2 \cos \theta_0 y R(\theta_0)} \sum_\mu \mathcal{A}_{\mu\gamma}, \quad (24)$$

where θ_0 is defined by the equation $q d = (2\eta_0)^{-1} \ln R(\theta_0)$ ($\eta_0 = \sin \theta_0$). Now for $\mathcal{T}_{\gamma,\theta < \theta_{th}}^{eff}$ we can write

$$\begin{aligned} \mathcal{T}_{\gamma,\theta < \theta_{th}}^{eff} &= \frac{15}{\pi^4} \left\langle \int_0^{q_c/q_T} dx \frac{x^3}{e^x - 1} \mathcal{T}_\gamma \right\rangle_{\theta < \theta_{th}} \\ &\approx \sum_\mu \frac{15}{\pi^4} \left\langle \int_0^{q_c/q_T} dx \frac{x^3}{e^x - 1} \mathcal{A}_{\mu\gamma} e^{2\eta q d} \right\rangle_{\theta < \theta_{th}} \\ &\quad \times \frac{\pi}{I} \frac{\delta(\theta - \theta_0)}{2 \cos \theta_0 y R(\theta_0)} \\ &= \sum_\mu \frac{15}{\pi^4} \frac{1}{dq_T} \\ &\quad \times \int_{x_{th}}^{q_c/q_T} dx \frac{x^3}{e^x - 1} \frac{\pi \mathcal{A}_{\mu\gamma}(\theta_0)}{I(\theta_0)} \frac{\sin \theta_0}{2 \cos \theta_0}. \end{aligned} \quad (25)$$

Here $x_{th} = \ln R(\theta_{th})/(2q_T d \sin \theta_{th})$. Let us further approximate (note that $\sin \theta_0 = \ln(R)/2xdq_T$)

$$\frac{\sin \theta_0}{\cos \theta_0} \approx \frac{\ln R(\theta_0)}{2xdq_T}, \quad (26)$$

when we obtain

$$\begin{aligned} \mathcal{T}_{\gamma,\theta < \theta_{th}}^{eff} &\approx \sum_\mu \frac{15}{\pi^4} \frac{1}{(2dq_T)^2} \\ &\quad \times \int_{x_{th}}^{q_c/q_T} dx \frac{x \pi f_{\mu\gamma}(\theta_0) \ln R(\theta_0)}{e^x - 1}, \end{aligned} \quad (27)$$

where $f_{\mu\gamma}(\theta_0) = \mathcal{A}_{\mu\gamma}(\theta_0)/I(\theta_0)$. Next we perform a Taylor series expansion for $f(\theta_0) = \mathcal{A}_{\mu\gamma}(\theta_0)/I(\theta_0)$ close to $\theta_0 = 0$:

$$\begin{aligned} f_{\mu\gamma}(\theta_0) &= \mathcal{A}_{\mu\gamma}(\theta_0)/I(\theta_0) \approx \theta_0^n \frac{f^n(0)}{n!} \\ &\approx \left(\frac{\ln(R(0))}{2dq_T x} \right)^n \frac{f^n(0)}{n!} \end{aligned} \quad (28)$$

where $f^n(0)$ is the first derivative that is non-zero. We find

$$\begin{aligned} \mathcal{T}_{\gamma,\theta < \theta_{th}}^{eff} &\approx \sum_\mu \frac{15}{\pi^3} \frac{[\ln R(0)]^{n+1}}{(2q_T d)^{2+n}} \\ &\quad \times \frac{f_{\mu\gamma}^n(0)}{n!} F_n\left(\frac{q_c}{q_T}, \theta_{th}\right), \end{aligned} \quad (29)$$

where $F_n(\frac{q_c}{q_T}, \theta_{th}) = \int_{x_{th}}^{q_c/q_T} dx \frac{x^{1-n}}{\exp(x) - 1}$.

B. Large angle contribution $\mathcal{T}_{\gamma,\theta > \theta_{th}}^{eff}$

At large angles only long wave length phonons participate, i.e., the phonon distribution can be approximated

by $N(\omega_{\mathbf{q}}, T) = [\exp(\hbar\omega_{\mathbf{q}}/k_B T) - 1]^{-1} \approx k_B T / \hbar\omega_{\mathbf{q}}$ and we find

$$\mathcal{T}_{\gamma, \theta > \theta_{th}}^{eff} \approx \frac{15}{\pi^4} \frac{1}{(q_T d)^3} \left\langle \int_0^{q_c d} dy y^2 \mathcal{T}_{\gamma}(y, \theta) \right\rangle_{\theta \geq \theta_{th}}. \quad (30)$$